π^+ Photoproduction from Hydrogen at Laboratory Energies from 589 to 1269 MeV*†

S. D. ECKLUND‡ AND R. L. WALKER
California Institute of Technology, Pasadena, California
(Received 15 February 1967)

The differential cross section for the reaction $\gamma+p\rightarrow\pi^++n$ was measured at 32 laboratory photon energies between 589 and 1269 MeV at the Caltech synchrotron. At each energy, data have been obtained at typically 15 π^+ angles between 6° and 90° in the center-of-mass (c.m.) system. A magnetic spectrometer was used to detect the π^+ photoproduced in a liquid-hydrogen target. Two Čerenkov counters were used to reject background of positrons and protons. The data clearly show the presence of a pole in the production amplitude due to one-pion exchange. Moravcsik fits to the angular distributions, including data from another experiment carried out by Thiessen, are presented. Extrapolation of these fits to the pole gives a value for the pion-nucleon coupling constant of 14.2±1.7, which is consistent with the accepted value. The "second" and "third" pion-nucleon resonances are evident as peaks in the total cross section and as changes in the shape of the angular distributions. At the third resonance, there is evidence for both a $D_{5/2}$ and an $F_{5/2}$ amplitude. The absence of large variations with energy in the 0° and 180° cross sections implies that the second and third resonances are mostly produced from an initial state with helicity $\frac{3}{2}$.

I. INTRODUCTION

THERE is currently considerable interest in detailed photoproduction data. Several authors have used the existing data to check sum rules.[1–3] The many resonant states found by phase-shift analysis[4–8] of πN scattering data open the question of whether these states are also photoproduced. A quark model[9] predicts the absence of the D_{15}(1652 MeV) and S_{11}(1715) resonant states in photoproduction from protons. Ideally, to check this prediction and to provide useful checks of sum rules, a complete multipole analysis of the data is desirable. Unfortunately, such an analysis involves a large number of parameters to be determined, so that detailed polarization data are required as well as data on the differential cross sections in order to obtain unique solutions. Some information can be obtained, however, from polynomial fits (in $\cos\theta$) to the angular distributions at fixed energies.

Of the various Feynman diagrams which might contribute to π^+ photoproduction, the one-pion exchange (OPE, commonly called the retardation term, the photoelectric term, or simply the π pole) is most evident in the data. Because it contributes a pole in the photoproduction amplitude close to the physical region at $\cos\theta=1/\beta$ (θ= c.m. π^+ production angle, β= c.m. pion velocity), it produces high powers of $\cos\theta$ in a polynomial expansion of the angular distribution. As would be expected, this makes it impossible to satisfactorily fit the data with a polynomial unless terms of very high order are included. On the other hand, a Moravcsik fit,[10] which allows for the pole denominator explicitly, works very well with a reasonable number of parameters. This fit separates the OPE contribution and consequently gives a measure of the pion-nucleon coupling constant. It also demonstrates the negative parity of the pion.

We report here the results of an experiment designed to explore in considerable detail the photoproduction of positive pions in the region from 6° to 90° in c.m. angle and from 589 to 1269 MeV. We combine our data with those of Thiessen[11] at larger angles in order to fit the angular distributions at each of 32 energies with Moravcsik fits. We thereby obtain numerous measurements of the coupling constant and information about the resonant states from the energy dependence of the coefficients of the fits. Section II gives the general experimental method, Sec. III discribes the apparatus, and Sec. IV gives pertinent information about the data collection and reduction to cross sections. Section V gives the results, Sec. VI, the discussion of the fits, and Sec. VII the conclusions drawn from the fits.

II. EXPERIMENTAL METHOD

The basic method employed in this experiment is similar to that used in a number of other photoproduction

* Work supported in part by the U. S. Atomic Energy Commission. Prepared under Contract AT(11-1)-68) for the San Francisco Operations Office, U. S. Atomic Energy Commission.

† This work is submitted by the first author in partial fulfillment of the requirements for the degree of Doctor of Philosophy at the California Institute of Technology.

‡ Present address: Stanford Linear Accelerator Center, P. O. Box 4393, Stanford, California 94305.

[1] A. Bietti, Phys. Rev. **142** 1258 (1966); **144**, 1289 (1966).

[2] S. L. Adler and F. J. Gilman, Phys. Rev. **152**, 1460 (1966); F. J. Gilman and H. J. Schnitzer, *ibid.* **150**, 1362 (1966).

[3] S. Fubini, G. Fulran, and C. Rossetti, Nuovo Cimento **40**, 1171 (1965).

[4] P. Bareyre, C. Brickman, A. V. Stirling, and G. Villet, Phys. Letters **18**, 342 (1965).

[5] L. D. Roper, R. M. Wright, and B. T. Feld, Phys. Rev. **138**, B190 (1965).

[6] B. H. Bransden, P. J. O'Donnel, and R. G. Moorhouse, Phys. Letters **11**, 339 (1964).

[7] P. Auvil, C. Lovelace, A. Donnachie, and A. T. Lea, Phys. Letters **12**, 76 (1964).

[8] J. Cence, Phys. Letters **20**, 306 (1966).

[9] R. G. Moorhouse, Phys. Rev. Letters **16**, 771 (1966).

[10] M. J. Moravcsik, Phys. Rev. **104**, 1451 (1956); J. G. Taylor, M. J. Moravcsik, and J. L. Uretsky, *ibid.* **113**, 689 (1959).

experiments.[11–18] Improvements in beam intensity and detection apparatus allowed us to measure the cross section for π^+ photoproduction in considerably greater detail than was achieved in earlier investigations.

The bremsstrahlung beam from the 1.5-GeV Caltech electron synchrotron illuminated a 3-in. liquid-hydrogen target. A magnetic spectrometer pivoted at the target was used to measure the yield of positively charged particles at a given angle and momentum. The spectrometer momentum aperture was divided into four parts so that measurements at four different momenta could be obtained simultaneously. Positrons, protons, and π^+ mesons were separated by two Čerenkov counters and, at lower momenta, by time of flight restrictions. The c.m. angle and energy are uniquely determined from the spectrometer angle and momentum by two-body kinematics for the reaction under investigation,

$$\gamma+p\rightarrow\pi^++n. \tag{1}$$

Background from multipion production was eliminated by kinematic constraints. For a given π^+ angle and momentum there is a minimum photon energy needed to produce an additional pion in the reactions

$$\gamma+p\rightarrow\pi^++\pi^0+n, \tag{2}$$

$$\gamma+p\rightarrow\pi^++\pi^-+p. \tag{3}$$

The synchrotron energy (end point of the bremsstrahlung spectrum) was kept below this threshold for three of the four momentum channels of the spectrometer Approximately one-third of the other channel overlapped the 2π threshold, but no significant yield was encountered for two reasons. First, the 2π production being a three-body final state contributes a π yield which increases slowly at threshold. Secondly, the 2π cross section is small at threshold,[19–21] not becoming large until the $\Delta(1238)$ resonance can be produced with a pion. Since the yield of π^- from hydrogen can come only from reaction (3) and other multipion states, measurement of this yield provides an easy way to estimate the multipion contamination. Such measurements of the π^- yield give an estimate of this background of less than 1% (see Fig. 2) as does an estimate based on the cross sections for reactions (2) and (3).

Contaminations of pions produced in other reactions were similarly eliminated by kinematic constraints and the maximum energy of the bremsstrahlung beam. Muons were presumed to come only from pion decay and no attempt was made to distinguish them from pions. The measured yields were corrected for the π^+ which decayed and the μ^+ from π^+ decay which were counted in the spectrometer.

III. APPARATUS AND CALIBRATION

A. Photon Beam and Hydrogen Target

The beam and target used in this experiment were as described in Ref. 11, with the exception of an additional collimator and sweep magnet present in this experiment. The bremsstrahlung beam was produced by monoenergetic electrons striking a 0.2 radiation-length tantalum target in the synchrotron, 10.4 m from the hydrogen target used in this experiment. The beam was collimated twice, before and after passing through a 6-in.-thick hydrogen target located upstream, and used in another experiment. A sweep magnet followed by a lead scraper (an aperture slightly larger than the primary photon beam) cleaned the beam of charged particles just before it entered the second hydrogen target used in this experiment.

The photon spectrum was calculated from a thick-target bremsstrahlung theory developed by Wolverton.[22] The accuracy of this calculation is estimated to be $\pm1.5\%$.

The beam was stopped and its total energy measured in a thick-plate ionization chamber, 10 m from the hydrogen target. Two auxiliary monitors, a thin-plate (0.005-in. Al) ionization chamber upstream from the hydrogen target and a two-counter telescope looking at the target at an angle of 90° to the beam, were also used to measure the beam. A Wilson quantameter[23] was used to calibrate the three monitors once a day. The consistency in the ratio of pairs of the three monitors allowed us to estimate the precision of the measurement of the beam energy. The fluctuating error in any one determination was found to be $\pm1.5\%$. This error was added, in quadrature, to the counting-statistical errors for each data run.

Approximately one year after the completion of our data taking, the quantameter was calibrated with a Faraday cup at the Stanford mark III linear accelerator.[24] This calibration agreed with the theoretical value

[11] H. A. Thiessen, Phys. Rev. **155**, 1488 (1967).
[12] F. P. Dixon and R. L. Walker, Phys. Rev. Letters **1**, 142 (1958); **1**, 358 (1958).
[13] J. H. Boyden, Ph.D. thesis, California Institute of Technology, 1962 (unpublished); R. L. Walker, in *Proceedings of the Xth International Conference on High Energy Physics at Rochester, 1960*, edited by E. C. G. Sudarshan, J. H. Tinlot, and A. C. Melissinos (Interscience Publishers, Inc., New York, 1961), p. 16.
[14] J. R. Kilner, Ph.D. thesis, California Institute of Technology, 1963 (unpublished).
[15] L. Hand and C. Schaerf, Phys. Rev. Letters **6**, 229 (1961).
[16] M. Heinberg, W. M. McClelland, F. Turkot, W. M. Woodward, R. R. Wilson, and D. M. Zipoy, Phys. Rev. **135**, B830 (1964).
[17] C. W. Peck, Phys. Rev. **135**, B830 (1963).
[18] M. Beneventano, R. Finzi, L. Mezzetti, L. Paoluzi, and S. Tazzari, Nuovo Cimento **28**, 1464 (1963).
[19] B. M. Chasen *et al.*, Phys. Rev. **119**, 811 (1960).
[20] J. V. Allaby, H. L. Lynch, and D. M. Ritson, Phys. Rev. **142**, 887 (1966).
[21] M. G. Hauser (private communication); also Phys. Rev. (to be published).
[22] An account of this work is in preparation. F. Wolverton provided a computer program for performing the calculations.
[23] R. R. Wilson, Nucl. Instr. Methods **1**, 101 (1957).
[24] H. A. Thiessen and J. Pine, California Institute of Technology Synchrotron Laboratory Internal Report No. 22 (unpublished).

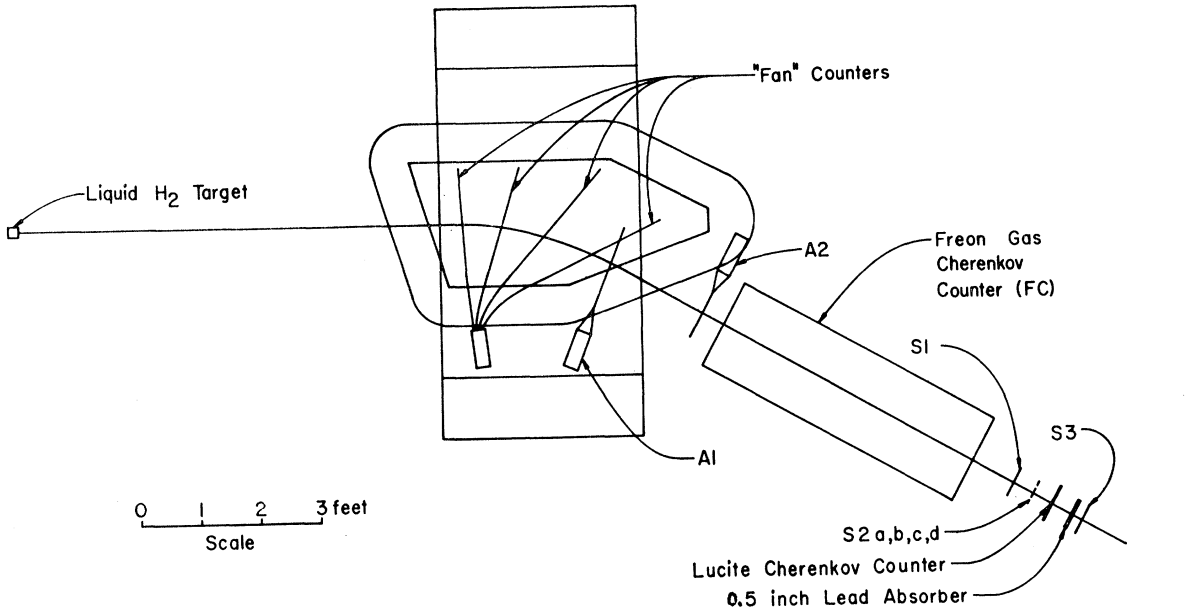

FIG. 1. A section through the vertical median plane of the spectrometer showing the locations of the counters.

to within 1.5%. We used the theoretical value of the calibration constant (4.80×10^{18} MeV/C at a temperature of 20°C and a pressure of 800 mm Hg) for our data reduction. The error is taken to be $\pm3\%$.

The liquid hydrogen in the target is contained in a cylindrical cup 3 in. in diameter made of 0.005-in. Mylar. The axis of the cup was vertical and perpendicular to the production plane defined by the beam and the spectrometer. The beam was 4.45 cm wide and 5.58 cm high at the target. The spectrometer was sensitive to the entire portion of the target illuminated by the beam. The target was cleaned occasionally to avoid the accumulation of condensible substances on the walls.

B. Spectrometer

The 1.2-GeV/c spectrometer used in this experiment deflected charged particles in a vertical plane by 27.3° with a radius of curvature of 105 in. The configuration of counters is shown in Fig. 1. Counters Al and S2a, b, c, d determine the solid angle and momentum acceptances. The absolute acceptances were calculated from accurate measurements of the fringe field in the median bending plane at two fields, 10 kG and 15 kG. These measurements directly yielded the acceptance in vertical angle and in momentum. The acceptance in horizontal angle was calculated from linear magnet theory. The solid-angle acceptance was $\Delta\Omega=1.35\times10^{-3}$ sr and the relative momentum acceptance was $\Delta P/P=0.024$ per channel. The total acceptances $\Delta\Omega\Delta P/P$ calculated from the measurements at the two fields differed by only 0.4%. The total acceptance was also calculated by linear magnet theory alone and the same answer was obtained to within 1%. The solid angle was checked directly by counting protons with an additional small counter in front of the magnet to define a known solid angle. This check was in agreement with the calculated solid angle within the 2% counting statistics.

The magnetic field of the spectrometer was set with a nuclear-magnetic-resonance system and was reproducible to better than 0.1%. The absolute momentum calibration of the central orbit was made by the floating-wire technique. The relation between momentum and magnetic field was found to depart from linearity due to saturation effects at fields above 8 kG, the magnitude of this deviation reaching 3.5% at 15 kG. The calibration was accurate to 0.1%; in actual data taking, however, uncertainties in the position of the momentum aperture and the mean position of the beam in the hydrogen target each add errors of 0.2% to this calibration. The central momentum at 10 and 15 kG was calculated from the fringe field measurements, and agreed with the floating-wire calibration to 0.1 and 0.2%, respectively.

It is possible to compare the spectrometer momentum calibration with the synchrotron energy meter by measuring the π^+ yield, at a fixed angle and momentum, as a function of the endpoint energy E_0, of the bremsstrahlung. When E_0 becomes less than the photon energy needed to produce a pion accepted by the spectrometer, the yield rapidly drops to zero with a slope determined by the bremsstrahlung shape and the spectrometer resolution. The yield in each of the four channels drops to zero at slightly different E_0 since each defines a different pion momentum and hence a different photon energy. In Fig. 2 we plot the yield from all four channels for a number of runs with each channel plotted at an effective E_0 shifted from the actual E_0 so as to account for their different defined photon energies. The abscissa

of Fig. 2 for the ith channel is

$$(\text{Effective } E_0)_i = E_0 - [K(p_i\theta_l) - K(p_0\theta_l)],$$

where $K(p,\theta_l)$ is the laboratory photon energy corresponding to single π^+ photoproduction at laboratory angle θ_l and laboratory momentum p, p_i is the mean momentum of the ith channel, and p_0 the central momentum of the magnet. Presenting the data in this form is reasonable only if the cross section changes slowly over the energy span of the four channels.

A comparison of the energy E_s indicated by the synchrotron energy meter, with the corresponding energy E_0 determined from the spectrometer calibration, was made by calculating the expected yields, properly folding in the energy resolution, for various assumed ratios of E_0/E_s, and comparing with the observed yields. Results from eight separate determinations at six different photon energies (settings of θ, p of the spectrometer) give an average $E_0/E_s = 1.005$ with an rms deviation of 0.004.

In reducing the data, we assumed our magnet calibration was correct; we consider it accurate to better than $\pm 0.5\%$. Because most of our data were taken at small angles, the absolute accuracy in photon energy is approximately the same, i.e., better than $\pm 0.5\%$. The energy of the synchrotron was taken to be $1.005E_s$ for consistency.

The spectrometer acceptance is complicated by the fact that some of the π^+ mesons decay before transversing the entire spectrometer. Since μ^+ are not distinguished from π^+ by the counters, they will also be counted. We have assumed direct μ^+ production to be negligible and we correct only for the μ^+ expected from π^+ decay. We used a Monte Carlo program to calculate the acceptance of the spectrometer for pions which decay to muons before reaching the last counter. This acceptance was calculated as a function of pion momentum and magnetic field, averaged over all other coordinates. A particular feature of this decay pion acceptance is that a π^+, which normally has too high a momentum to be accepted, can decay to a μ^+ somewhere in the spectrometer and be counted, so that the decay pion acceptance has a long high-momentum tail. The cutoff of this tail is provided by the maximum energy of the bremsstrahlung. Typical fractional corrections for pion decay are given in Table I.

TABLE I. π^+ decay correction.

Momentum (MeV/c)	Fraction of pions which decay	Muons counted[a]	Fractional correction
500	0.214	0.072	0.142
600	0.182	0.063	0.119
700	0.159	0.054	0.105
800	0.140	0.047	0.093
900	0.125	0.041	0.084
1000	0.113	0.037	0.076
1100	0.104	0.034	0.070
1200	0.096	0.032	0.064

[a] The muons counted are expressed as a fraction of the number of pions which would have been counted if pions did not decay.

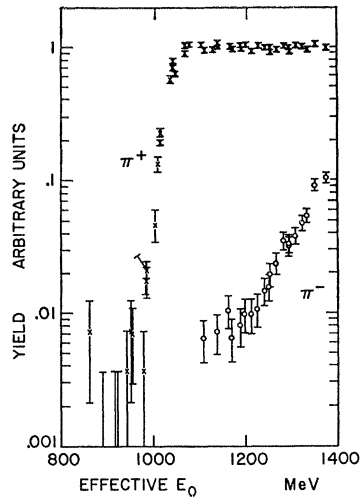

FIG. 2. Measured π^+ and π^- yields from hydrogen as a function of the bremsstrahlung end-point energy. Empty target backgrounds have not been subtracted from the yields. The spectrometer was set at 23° lab and a momentum of 925 MeV/c.

C. Counters and Electronic Logic

Two Čerenkov counters were used to distinguish π^+ from protons and positrons. A Plexiglas Čerenkov counter LC (Fig. 1) was used to separate protons from π^+ and e^+. It was 1.5 in. thick and wrapped with nonreflective paper, so that only light which internally reflects can reach the photomultiplier tubes. This determines its velocity threshold of $\beta = 0.90$. Over the range of momentum used (490–1260 MeV/c), pions have β in the range 0.96 to 0.99 whereas protons have β in the range 0.46 to 0.80. The efficiency of LC was measured and found to be $0.3 \pm 0.3\%$ for protons and $98.4 \pm 0.4\%$ for pions. In the most unfavorable case encountered while measuring cross sections, the yield before discrimination consisted of three times as many protons as pions.

A threshold Freon Čerenkov counter FC was used to identify positrons. It had a radiator consisting of 60 in. of Freon-12 at atmospheric pressure. A spherical plastic mirror reflected the Čerenkov light into a 5-in. phototube. Its velocity threshold was $\beta = 0.999$ and, consequently, it counted only positrons for the momentum range used. A 0.5-in. thickness of lead stopped very low energy electrons that resulted from conversion of γ rays in the first aperture counter or elsewhere. The efficiency of FC for counting positrons was measured and found to be better than 99.8%. The largest positron yield encountered while measuring cross sections was three times the pion yield (before discrimination).

The scintillation counters defined the spectrometer acceptance, provided time-of-flight measurements, and eliminated accidental coincidences. Two fan counters, each consisting of four long pieces of scintillators fast-

ened to a pole face of the magnet, were used to veto events scattering off the magnet pole faces. This veto rate varied from 9% at a momentum of 500 MeV/c to 3% at 1200 MeV/c .For cross sections measured at c.m. angles less than 20°, the fan counters could not be used due to high count rates. These small-angle measurements were corrected according to the expected veto rate as determined from measured rates at larger angles.

The electronic logic was set up to count the pion rate and one other monitor rate which could be chosen at will. Usually the proton rate, the electron rate, or the efficiency of the last counter was chosen as the additional monitor. The logic was split into several levels, characterized by increasing resolving times. The first level generated signals from 4- to 6-nsec coincidences between the pairs A1·S1, A2·S1, and Fan·S1. These were then combined in slower 50-nsec coincidences to define particle yields. The total particle yield in the ith spectrometer channel was defined as

$$\Sigma_i=(\mathrm{A1}\cdot\mathrm{S1})\cdot(\mathrm{A2}\cdot\mathrm{S1})\cdot(\mathrm{Fan}\cdot\mathrm{S1})^a\cdot\mathrm{S2}_i\cdot\mathrm{S3},$$

where the superscript a means an anticoincidence. The π^+, proton, and positron yields are then, respectively,

$$\pi_i=\Sigma_i\cdot\mathrm{LC}\cdot(\mathrm{FC})^a,$$
$$p_i=\Sigma_i\cdot(\mathrm{LC})^a\cdot(\mathrm{FC})^a,$$
$$e_i=\Sigma_i\cdot\mathrm{LC}\cdot\mathrm{FC}.$$

At low momenta, below 800 MeV/c, the fast timing requirements automatically eliminated protons from the Σ yield. In addition to scaling the π counts, the single counter rates and the fast coincidence rates were monitored to check the operation of all parts of the detection system. Pulse-height spectra were monitored one at a time while taking data to check phototube gains and discriminator bias settings. No correction for dead time or accidental coincidences was necessary. The π rate was corrected to account for the proton and pion efficiency of LC.

IV. DATA COLLECTION AND REDUCTION

The π^+ yield was obtained at four momenta and one angle for each setting of the spectrometer and bremsstrahlung end point. Three-hundred runs at 129 different settings were taken, resulting in 516 cross-section measurements. The length of a typical run varied from $\frac{1}{2}$ to 2 h, depending on the setting and available beam intensity. The data were collected in three running periods of about 2, 4, and 2 months, over a total of about 2 yr.

The cross-section data were taken with the bremsstrahlung endpoint E_0 nominally set 130 MeV above the photon energy defined by the central spectrometer momentum. This corresponds to $E_0=1148$ MeV for the momentum and angle in Fig. 2. Notice the π^+ yield just below threshold is $\leq 1\%$ of the normal yield, providing proof of good identification of π^+ mesons. Cross-section measurements were made with eight values of E_0. At each E_0, settings of angle and momentum were chosen to give c.m. angles from 6° to 90° at a constant mean-photon energy. At each setting, data at four energies were recorded corresponding to the four spectrometer channels. In this way, 32 angular distributions were obtained.

Because the momentum apertures are fixed, the separation of the four photon energies increases slightly with angle so that the angular distributions obtained are at only approximately constant energies. In order to present angular distributions at constant energies, the data points were interpolated in energy by the following scheme. For each setting, the four cross sections were fitted with a quadratic in photon energy. Each data point was then moved to the desired energy by changing the observed value of the cross section by the same amount the quadratic fit changes over the distance moved. For most of the data, namely for c.m. angles less than 50°, the distance moved was always less than 0.6% in laboratory photon energy. In the worst case, at 90°, the move was 3.3%. The advantage of this method is that the data are not artificially smoothed by the interpolating process. The error assigned to the interpolated cross section is taken to be the same as that of the original point; the additional error due to the uncertainty in the change of the fit is negligible.

The π^+ yields from hydrogen were calculated from the difference in the measured π^+ yield between runs with a full target and an empty target. The empty-target yield varied from 13% of the full-target yield at 3.5° lab. to 4% at 30°.

The measured yields were corrected for nuclear absorption and multiple scattering in the spectrometer by two methods. For matter near the end of the spectrometer flight path (counters S1, S2, LC, and the 0.5 in. of lead), direct measurements of losses as a function of momentum with additional absorbers were used to correct for both absorption and multiple-scattering losses. For the remaining matter, a geometric nuclear cross section was used, independent of momentum, of the form $\sigma=CA^{2/3}$ for an element with atomic number A. The constant C was determined from measurements of losses with thick Plexiglas absorbers to be $C=35.3\pm4.2$ mb. The total correction factor varied linearly with momentum, from 0.132 at 500 MeV/c to 0.095 at 1200 MeV/c. The uncertainty in this correction is ±0.02.

For purposes of calculating the cross section, an integral over energy was performed for each data point. The spectrometer resolution functions, modified to account for pion decay and broadened by 7 MeV/c to account for multiple scattering, were folded into the bremsstrahlung spectrum. The energy dependence was treated with this amount of detail to avoid introducing a false systematic dependence upon spectrometer channel.

TABLE II. The measured values of the differential cross sections in μb/sr and the associated standard deviation errors Δ. The π^+ c.m. angle is θ. The laboratory photon energy k is in MeV.

θ (deg)	σ (μb/sr)	Δ (μb/sr)	θ (deg)	σ (μb/sr)	Δ (μb/sr)	θ (deg)	σ (μb/sr)	Δ (μb/sr)	θ (deg)	σ (μb/sr)	Δ (μb/sr)
	$k=589$			$k=603$			$k=618$			$k=635$	
6.04	17.88	0.76	6.08	16.69	0.71	6.12	18.84	0.74	6.16	17.34	0.70
8.02	16.37	0.71	8.07	18.22	0.72	8.12	17.46	0.69	8.18	16.27	0.66
10.14	15.62	0.51	10.21	15.71	0.48	10.27	15.38	0.48	10.35	15.70	0.48
12.11	14.88	0.64	12.18	14.36	0.61	12.26	14.31	0.60	12.35	14.50	0.59
14.07	13.37	0.45	14.16	13.59	0.45	14.25	13.13	0.43	14.35	13.82	0.44
16.04	13.21	0.55	16.14	12.58	0.52	16.25	13.49	0.53	16.36	12.49	0.50
20.00	11.93	0.49	20.12	11.42	0.48	20.25	11.34	0.47	20.39	10.83	0.44
24.96	11.38	0.58	25.11	11.11	0.56	25.26	11.08	0.55	25.44	11.50	0.55
29.93	11.12	0.48	30.11	11.09	0.46	30.29	10.43	0.45	30.50	10.96	0.45
34.90	10.07	0.56	35.11	11.74	0.58	35.31	10.85	0.55	35.55	10.83	0.54
39.86	10.60	0.31	40.09	10.58	0.31	40.33	10.97	0.30	40.59	10.76	0.30
49.83	10.30	0.57	50.09	9.49	0.55	50.38	11.20	0.57	50.70	10.61	0.56
59.79	10.01	0.42	60.09	10.15	0.42	60.42	10.27	0.42	60.78	10.53	0.42
	$k=647$			$k=663$			$k=680$			$k=698$	
6.06	18.87	0.57	6.10	18.18	0.54	6.14	18.44	0.53	6.18	16.55	0.49
8.02	16.16	0.51	8.08	17.86	0.52	8.13	15.82	0.49	8.19	16.28	0.48
10.16	15.85	0.41	10.22	15.55	0.40	10.29	16.46	0.40	10.37	15.05	0.38
12.10	14.82	0.39	12.18	14.51	0.38	12.27	13.97	0.36	12.36	14.08	0.36
14.07	14.40	0.40	14.16	13.72	0.39	14.26	13.59	0.38	14.37	13.29	0.37
16.04	13.51	0.41	16.15	12.96	0.39	16.26	12.31	0.38	16.38	12.68	0.38
19.99	11.95	0.35	20.12	11.69	0.34	20.26	12.30	0.34	20.40	11.31	0.32
24.94	10.76	0.33	25.11	11.03	0.33	25.27	11.26	0.32	25.46	11.06	0.31
29.91	11.17	0.33	30.11	10.92	0.32	30.30	11.23	0.33	30.52	11.21	0.32
39.85	11.19	0.23	40.09	11.49	0.23	40.36	11.76	0.23	40.63	11.70	0.23
49.79	11.73	0.36	50.09	11.60	0.35	50.39	12.17	0.35	50.72	11.85	0.34
59.77	10.96	0.36	60.09	11.33	0.35	60.45	10.95	0.34	60.81	11.35	0.35
69.73	9.97	0.32	70.09	10.10	0.31	70.47	10.70	0.32	70.87	10.38	0.31
79.71	8.50	0.27	80.08	8.45	0.27	80.48	8.91	0.27	80.89	8.93	0.27
	$k=715$			$k=733$			$k=752$			$k=772$	
6.05	17.28	0.67	6.09	14.92	0.61	6.14	13.53	0.58	6.19	14.33	0.56
8.01	14.56	0.61	8.07	14.14	0.59	8.13	14.53	0.57	8.19	13.44	0.54
10.16	14.85	0.47	10.23	13.45	0.45	10.31	12.50	0.41	10.39	11.68	0.40
12.11	13.95	0.45	12.20	12.13	0.42	12.29	11.69	0.40	12.38	11.49	0.39
14.07	12.72	0.43	14.17	11.80	0.41	14.27	11.32	0.39	14.39	9.97	0.36
16.05	12.85	0.37	16.16	11.17	0.34	16.28	10.09	0.32	16.40	9.59	0.31
19.99	11.19	0.41	20.13	10.34	0.38	20.28	9.61	0.36	20.43	9.03	0.34
24.94	10.20	0.53	25.11	9.54	0.50	25.29	9.71	0.49	25.48	8.58	0.46
29.90	11.27	0.48	30.10	10.16	0.45	30.32	9.11	0.41	30.54	8.43	0.39
34.86	10.50	0.55	35.09	9.64	0.51	35.34	8.87	0.48	35.60	8.78	0.47
39.83	11.70	0.34	40.10	10.53	0.31	40.37	9.54	0.29	40.66	8.71	0.27
49.77	11.79	0.61	50.08	10.63	0.55	50.42	10.08	0.52	50.76	8.63	0.47
59.74	11.67	0.61	60.09	9.99	0.55	60.46	9.60	0.52	60.85	7.98	0.45
69.70	10.83	0.60	70.09	10.74	0.58	70.49	9.38	0.52	70.91	7.90	0.45
79.68	9.66	0.31	80.08	9.20	0.29	80.50	7.99	0.26	80.94	6.85	0.23
	$k=793$			$k=813$			$k=834$			$k=857$	
6.06	14.51	0.54	6.10	14.41	0.51	6.15	14.14	0.50	6.20	13.28	0.47
8.02	12.67	0.49	8.08	13.06	0.49	8.15	13.34	0.48	8.21	12.22	0.45
10.18	12.25	0.30	10.25	12.01	0.29	10.33	11.24	0.27	10.42	11.16	0.26
12.12	10.98	0.40	12.21	11.36	0.39	12.31	10.81	0.37	12.41	10.28	0.36
14.07	10.17	0.27	14.18	10.67	0.26	14.29	9.88	0.25	14.41	9.64	0.24
16.04	9.66	0.37	16.16	9.45	0.35	16.29	8.87	0.33	16.42	8.70	0.32
18.01	9.60	0.36	18.15	9.39	0.35	18.29	8.20	0.32	18.44	8.33	0.32
19.99	8.86	0.26	20.14	8.37	0.25	20.29	7.88	0.24	20.47	8.38	0.24
24.94	8.71	0.42	25.12	8.69	0.41	25.31	7.66	0.38	25.52	8.05	0.38
29.88	8.28	0.25	30.10	8.16	0.24	30.32	7.73	0.22	30.57	7.43	0.22
34.86	7.64	0.33	35.10	7.94	0.33	35.37	7.36	0.31	35.65	7.63	0.31
39.83	7.88	0.13	40.10	7.45	0.12	40.39	7.05	0.12	40.70	6.88	0.11
49.75	7.09	0.21	50.08	6.35	0.19	50.43	5.90	0.18	50.80	5.80	0.18
59.71	6.30	0.32	60.08	5.50	0.28	60.47	4.98	0.27	60.89	4.90	0.26
69.68	5.72	0.22	70.08	4.80	0.20	70.50	4.04	0.17	70.96	3.58	0.16
79.67	5.64	0.32	80.09	4.36	0.27	80.52	3.99	0.25	80.99	3.09	0.21
	$k=880$			$k=902$			$k=926$			$k=951$	
6.05	13.88	0.42	6.10	12.30	0.38	6.15	12.37	0.37	6.20	10.76	0.35
8.00	11.70	0.48	8.06	11.53	0.45	8.13	10.80	0.43	8.20	8.84	0.38
10.16	10.64	0.39	10.24	10.38	0.38	10.32	9.69	0.35	10.41	8.22	0.32
12.11	10.55	0.28	12.21	9.60	0.26	12.31	9.62	0.25	12.41	8.69	0.23
14.07	9.55	0.37	14.18	9.34	0.36	14.30	8.48	0.32	14.42	7.74	0.31

TABLE II. (*continued.*)

θ (deg)	σ (μb/sr)	Δ (μb/sr)	θ (deg)	σ (μb/sr)	Δ (μb/sr)	θ (deg)	σ (μb/sr)	Δ (μb/sr)	θ (deg)	σ (μb/sr)	Δ (μb/sr)
	$k=880$			$k=902$			$k=926$			$k=951$	
16.06	9.32	0.25	16.18	8.47	0.24	16.31	8.31	0.23	16.44	7.90	0.22
19.98	8.42	0.34	20.12	8.17	0.33	20.29	8.10	0.33	20.46	8.08	0.32
29.87	7.92	0.24	30.10	8.43	0.24	30.33	7.92	0.23	30.59	8.10	0.23
39.80	7.25	0.14	40.09	7.81	0.14	40.40	7.92	0.14	40.72	8.41	0.15
49.74	6.51	0.22	50.08	6.81	0.22	50.45	6.93	0.23	50.83	7.57	0.24
59.68	4.89	0.23	60.06	5.12	0.23	60.48	5.28	0.23	60.90	5.34	0.23
69.64	3.31	0.24	70.07	3.39	0.24	70.52	3.59	0.24	70.98	3.74	0.25
79.62	2.69	0.23	80.06	2.70	0.23	80.53	2.89	0.22	81.01	2.54	0.20
	$k=977$			$k=1002$			$k=1028$			$k=1056$	
6.06	9.95	0.26	6.11	9.37	0.24	6.17	7.76	0.21	6.22	7.45	0.20
8.02	9.22	0.34	8.09	7.99	0.31	8.16	7.52	0.29	8.23	6.81	0.27
10.19	8.23	0.25	10.27	7.17	0.22	10.36	6.92	0.21	10.45	6.00	0.19
12.12	8.20	0.19	12.22	6.98	0.17	12.32	6.59	0.16	12.44	5.69	0.15
14.09	7.95	0.22	14.21	7.33	0.20	14.33	6.95	0.19	14.46	5.92	0.17
16.04	8.00	0.22	16.17	7.40	0.20	16.31	6.90	0.19	16.45	6.14	0.18
19.98	7.55	0.23	20.15	7.56	0.23	20.32	6.98	0.21	20.49	6.72	0.21
24.92	8.64	0.14	25.13	8.62	0.13	25.33	8.43	0.13	25.55	7.78	0.12
29.86	8.94	0.20	30.10	8.80	0.20	30.34	8.81	0.19	30.60	8.00	0.18
34.82	9.42	0.18	35.09	9.47	0.18	35.37	9.49	0.17	35.67	8.24	0.16
39.77	9.51	0.12	40.08	9.44	0.12	40.39	9.37	0.12	40.72	8.67	0.11
44.75	9.38	0.20	45.09	9.51	0.20	45.43	9.50	0.20	45.79	8.49	0.18
49.71	8.39	0.26	50.07	8.25	0.25	50.44	8.15	0.24	50.84	7.56	0.23
54.69	7.38	0.20	55.07	8.08	0.21	55.47	7.70	0.20	55.90	6.72	0.17
59.66	6.81	0.23	60.07	6.42	0.22	60.49	6.12	0.21	60.94	5.68	0.20
64.64	5.64	0.18	65.07	5.75	0.18	65.51	5.68	0.17	65.98	4.96	0.15
69.61	4.75	0.10	70.06	4.61	0.09	70.52	4.52	0.09	71.01	4.01	0.08
74.60	3.58	0.15	75.06	4.01	0.15	75.53	3.64	0.14	76.03	3.41	0.13
79.59	2.89	0.15	80.05	3.04	0.15	80.53	2.78	0.13	81.04	2.56	0.12
84.59	2.38	0.13	85.06	2.42	0.13	85.54	2.24	0.12	86.05	2.09	0.11
89.58	2.15	0.08	90.05	2.04	0.07	90.54	2.02	0.07	91.06	1.74	0.06
	$k=1074$			$k=1102$			$k=1131$			$k=1162$	
6.06	7.03	0.21	6.11	6.48	0.20	6.17	5.51	0.17	6.22	5.34	0.17
8.03	6.38	0.20	8.09	5.34	0.17	8.17	4.95	0.16	8.24	4.49	0.15
10.20	5.83	0.16	10.28	5.31	0.14	10.38	4.48	0.13	10.47	4.03	0.12
12.13	5.75	0.15	12.24	5.16	0.14	12.35	4.64	0.13	12.46	4.13	0.12
14.08	5.92	0.20	14.20	5.28	0.18	14.32	5.13	0.18	14.46	4.45	0.16
16.04	5.99	0.15	16.18	5.48	0.14	16.32	4.77	0.13	16.48	4.17	0.12
19.99	6.58	0.16	20.16	5.84	0.15	20.34	4.92	0.13	20.52	4.52	0.13
24.92	7.54	0.18	25.13	6.41	0.16	25.34	5.37	0.14	25.58	5.05	0.13
29.85	7.38	0.13	30.10	6.52	0.12	30.36	5.67	0.11	30.63	5.02	0.10
34.81	8.19	0.15	35.10	6.43	0.13	35.39	5.52	0.11	35.70	4.72	0.10
39.77	8.28	0.08	40.08	6.81	0.07	40.41	5.62	0.06	40.76	4.73	0.06
44.73	8.08	0.17	45.09	6.39	0.15	45.45	5.20	0.13	45.83	4.42	0.12
49.70	7.29	0.18	50.08	6.03	0.16	50.47	4.75	0.13	50.89	3.82	0.12
54.67	6.77	0.17	55.08	5.28	0.14	55.49	4.42	0.12	55.94	3.33	0.10
59.64	5.44	0.10	60.08	4.24	0.09	60.51	3.39	0.07	60.98	2.60	0.06
64.61	4.63	0.14	65.06	3.95	0.12	65.52	2.91	0.10	66.01	2.20	0.08
69.59	3.83	0.08	70.05	3.03	0.07	70.53	2.43	0.06	71.04	1.82	0.05
74.57	2.80	0.15	75.06	2.47	0.13	75.55	1.68	0.10	76.07	1.38	0.09
79.56	2.51	0.13	80.05	1.91	0.11	80.55	1.68	0.09	81.08	1.19	0.08
84.56	1.86	0.13	85.06	1.55	0.11	85.57	1.26	0.10	86.10	1.03	0.09
89.55	1.69	0.11	90.05	1.32	0.09	90.56	1.21	0.08	91.09	0.89	0.07
	$k=1174$			$k=1204$			$k=1235$			$k=1269$	
6.08	5.80	0.30	6.13	5.01	0.26	6.19	4.76	0.25	6.25	4.38	0.24
8.03	4.70	0.20	8.10	4.15	0.19	8.17	3.76	0.17	8.25	3.29	0.16
10.22	4.64	0.17	10.31	4.16	0.16	10.40	3.73	0.14	10.50	3.29	0.14
12.15	4.39	0.27	12.26	4.09	0.25	12.37	3.48	0.24	12.49	3.31	0.22
14.10	3.91	0.25	14.22	4.10	0.24	14.36	3.84	0.23	14.49	3.46	0.22
16.07	4.44	0.19	16.21	3.92	0.17	16.36	3.81	0.17	16.52	3.37	0.16
20.01	4.18	0.25	20.18	4.13	0.24	20.36	3.99	0.23	20.55	4.15	0.24
24.94	5.30	0.30	25.15	4.52	0.27	25.37	4.58	0.27	25.61	4.63	0.26
29.87	5.13	0.40	30.12	5.21	0.38	30.38	4.01	0.33	30.66	3.90	0.33
34.82	4.38	0.37	35.11	4.77	0.37	35.41	4.00	0.34	35.73	4.46	0.36
39.79	4.69	0.14	40.12	3.96	0.12	40.45	3.78	0.12	40.81	3.67	0.11
49.71	3.85	0.21	50.09	3.24	0.20	50.50	2.74	0.17	50.92	2.52	0.17
59.66	2.63	0.22	60.09	1.98	0.19	60.53	1.98	0.18	61.02	1.57	0.16
69.62	1.48	0.17	70.09	1.62	0.17	70.57	1.07	0.13	71.09	1.09	0.14
79.59	1.06	0.16	80.08	0.95	0.14	80.59	0.65	0.11	81.14	0.62	0.12
89.58	0.68	0.07	90.09	0.71	0.07	90.60	0.56	0.06	91.15	0.57	0.06

V. RESULTS

The measured cross sections, interpolated in energy to provide angular distributions, are given in Table II. Uninterpolated cross sections are available in Ref. 25. As a sample, 14 of the 32 angular distributions, including data from the experiment of Thiessen,[11] are shown in Fig. 3. The curves are Moravcsik-equivalent fits with eight parameters and a fixed π-N coupling constant of 14.7. To illustrate the over-all shape of the cross section as a function of energy and angle, the fitted curves from all 32 energies are displayed in an isometric view in Fig. 4.

The results of this experiment are compared with earlier measurements in Fig. 5. The smooth curves are the fits obtained in this experiment. In most cases the agreement is satisfactory. The agreement between this experiment and that of Thiessen was checked at places where the data overlapped. The Moravcsik-equivalent fits were repeated with a variable normalization factor for the data of one experiment relative to the other. The average best-normalization factor differed from unity by $3\pm3\%$, the cross section from this experiment being the larger. This difference was not considered significant and no normalization factor was included in the fits presented here.

A complete set of graphs similar to those in Fig. 3 and Fig. 5 is given in Refs. 25 and 26. The cross sections from Thiessen were interpolated to appropriate energies. The values used are tabulated in Ref. 26.

The errors quoted with the cross sections are standard deviations resulting from counting statistics and a 1.5% beam monitoring fluctuation added in quadrature for each run. The constant or slowly varying errors are listed in Table III. The error in c.m. angle is less than 0.05° for any point. The calibration of the laboratory photon energy is considered consistent between points to better than 0.2% and accurate over all to 0.5%.

The rms energy resolution in laboratory photon energy varies from 1.4 to 2.5%, depending upon angle and energy. The angular resolution is typically 0.8° rms in c.m. angle. The error in measured cross section due to the finite resolution in angle and energy was estimated for extreme cases to be less than 0.3 and 2%, respectively.

TABLE III. Systematic errors.

Source	Error (%)
Decay correction	1.0
Magnet acceptance	1.0
Absorption correction	2.0
Absolute beam calibration	3.0
Counter efficiencies	0.5
Target density and thickness	1.0
Bremsstrahlung shape	1.5
Quadrature sum	4.3
Absolute sum	10.0

[25] S. D. Ecklund, Ph.D. thesis, California Institute of Technology, 1966 (unpublished).

[26] J. T. Beale, S. D. Ecklund, and R. L. Walker, California Institute of Technology Synchrotron Laboratory Report No. CTSL-42, 1966 (unpublished).

VI. FITS TO THE ANGULAR DISTRIBUTIONS

A. Phenomenology and Moravcsik Fits

Contributions to the π^+ photoproduction amplitude may be classified according to three types of Feynman diagrams. These represent meson exchange, baryon or resonance exchange, and baryon or resonance intermediate state. The first type, meson exchange, produces poles in the amplitude beyond the physical region near small π^+ production angles. The second type, baryon or resonance exchange, produces poles beyond the physical region near 180°. In the third type, an intermediate state may show up as a resonance at an energy equal to the mass of the intermediate particle. While all of the three types of diagrams, each with several intermediate or exchanged particles, contribute to the photoproduction amplitude, the π meson exchange (OPE) is especially noticeable. The pole produced by it is extremely close to the physical region, at $\cos\theta=1/\beta \approx 1.063-1.023$, for the region of laboratory photon energy 589–1269 MeV. Poles resulting from other known exchanges are much farther from the physical region and the amplitude due to them may be approximated by a polynomial in $\cos\theta$. For example, ρ meson exchange produces a pole at $\cos\theta=2.33$ at a laboratory photon energy of 800 MeV. We desire, therefore, to separate the OPE amplitude from the total amplitude and treat it explicitly.

In addition to studying features which may be ascribed to the one-pion exchange amplitude, we are interested in learning as much as possible about the intermediate states, especially resonances, which contribute to the photoproduction process. In order to do this, we must be careful to analyze the angular distributions in such a way that effects of these intermediate states are not entirely obscured by the OPE amplitude. For this purpose, we shall write the photoproduction amplitude, with the OPE contribution explicitly separated as indicated above, in the helicity formalism of Jacob and Wick.[27]

There are eight helicity amplitudes $A_{\mu\lambda}(\theta,\phi)$ for pion photoproduction corresponding to four values of the initial helicity λ and two values of the final helicity μ. ($\lambda=\lambda_\gamma-\lambda_1$ and $\mu=-\lambda_2$, where λ_γ, λ_1, and λ_2 are the helicities of the incident photon, the initial nucleon, and the final nucleon, respectively, in the c.m. system.) Only four of the eight amplitudes are independent because parity symmetry imposes the relations[27]

$$A_{-\mu,-\lambda}(\theta,\phi)=-e^{i(\lambda-\mu)(\pi-2\phi)}A_{\mu,\lambda}(\theta,\phi). \quad (4)$$

[27] M. Jacob and G. C. Wick, Ann. Phys. (N. Y.) 7, 404 (1959).

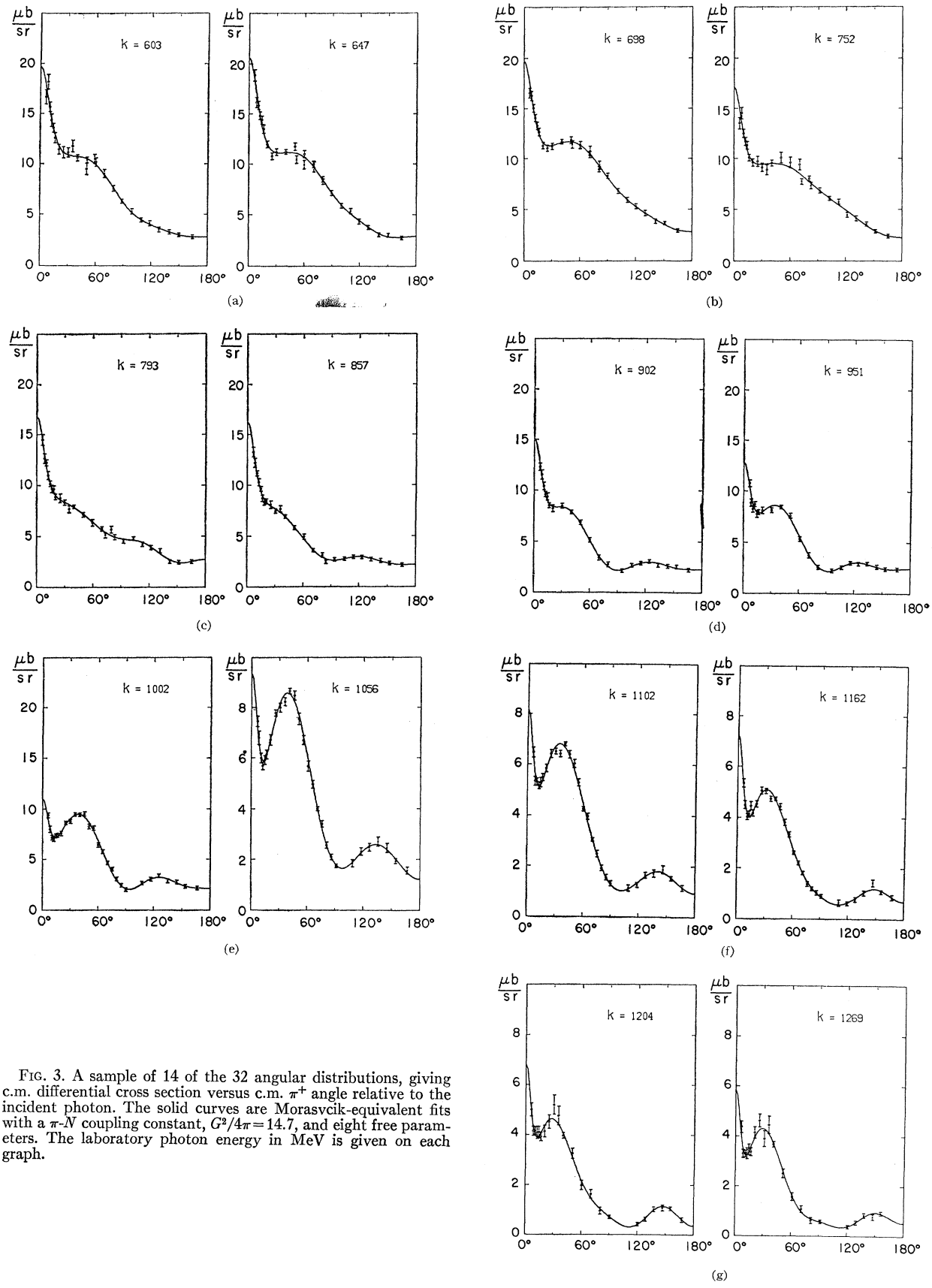

FIG. 3. A sample of 14 of the 32 angular distributions, giving c.m. differential cross section versus c.m. π^+ angle relative to the incident photon. The solid curves are Morasvcik-equivalent fits with a π-N coupling constant, $G^2/4\pi = 14.7$, and eight free parameters. The laboratory photon energy in MeV is given on each graph.

We choose as the four independent amplitudes those with $\lambda_\gamma=+1$, and designate these $H_n(\theta,\phi)$ as follows:

$$H_1=A_{1/2,3/2}, \quad H_2=A_{1/2,1/2}, \qquad (5)$$
$$H_3=A_{-1/2,3/2}, \quad H_4=A_{-1/2,1/2}.$$

Using this notation, and separating the OPE amplitude from all other contributions, we write the differential cross section in the form

$$\sigma(\theta)=\frac{1}{2}\frac{q}{k}\sum_{n=1}^{4}|H_n^{\rm OPE}+H_n|^2, \qquad (6)$$

where k and q are the momenta of the incident photon and the outgoing pion, respectively. The OPE helicity amplitudes in the c.m. system are

$$H_1^{\rm OPE}=(1/\sqrt{2})e^{i\phi}\sin\theta\cos\tfrac{1}{2}\theta\,F_-,$$
$$H_2^{\rm OPE}=-(1/\sqrt{2})\sin\theta\sin\tfrac{1}{2}\theta\,F_+, \qquad (7)$$
$$H_3^{\rm OPE}=-(1/\sqrt{2})e^{2i\phi}\sin\theta\sin\tfrac{1}{2}\theta\,F_+,$$
$$H_4^{\rm OPE}=-(1/\sqrt{2})e^{i\phi}\sin\theta\cos\tfrac{1}{2}\theta\,F_-,$$

where

$$F_\pm=\frac{e\sqrt{2}G}{4\pi}\frac{1}{2W}\frac{\beta}{1-\beta\cos\theta}\times\left[\left(\frac{E_2+M_2}{E_1+M_1}\right)^{1/2}\pm\left(\frac{E_2-M_2}{E_1-M_1}\right)^{1/2}\right],$$

$e^2/4\pi=1/137$,

$G^2/4\pi=\pi$-N coupling constant (≈ 14.7),

$W=$ total energy,

$\beta=$ velocity of π^+,

$\theta=\pi^+$ production angle,

$E_1=$ initial nucleon total energy,

$E_2=$ final nucleon total energy,

$M_1=$ initial nucleon mass,

$M_2=$ final nucleon mass.

We should remark that although $H_n^{\rm OPE}$ is not gauge-invariant by itself, it differs from the complete electric Born approximation which is gauge-invariant only by S and P waves, and these can be absorbed in H_n.

The cross section resulting from the OPE amplitudes alone is

$$\sigma_{\rm OPE}(\theta)=\frac{1}{2}\frac{q}{k}\sum_n|H_n^{\rm OPE}|^2,$$

$$\sigma_{\rm OPE}(\theta)=\frac{e^2G^2}{(4\pi)^2}\frac{q}{k}\frac{1}{4W^2}\frac{\beta^2\sin^2\theta}{2k^2(1-\beta\cos\theta)^2}\times[(M_2-M_1)^2-m^2+2k\omega(1-\beta\cos\theta)], \qquad (8)$$

where m is the π^+ mass and ω is the π^+ total energy.

In what follows, we shall assume that a partial-wave expansion of the amplitudes H_n contains only angular momenta j up to some upper limit m. This is exact for intermediate-state diagrams, provided m is as large as the spin of the intermediate particle or resonance. For the meson and baryon exchanges present in H_n, this is an approximation; we neglect the partial waves with $j>m$ which may be present in small amounts. We wish to specify a state by its total angular momentum and parity. A state of definite parity is a combination of the two final helicity states so we must give up the final helicity label. We may retain, however, a definite initial helicity at the expense of mixing electric and magnetic multipoles. We shall use "helicity elements" $A_{l\pm}$ and $B_{l\pm}$[28]; where l specifies the π-N orbital angular momentum [and parity $=-(-1)^l$], the total angular momentum is $j=l\pm\frac{1}{2}$, and the initial helicity is $\frac{1}{2}$ for $A_{l\pm}$ and $\frac{3}{2}$ for $B_{l\pm}$. With this notation, the partial-wave expansion of the helicity amplitudes is given by

$$H_1=\frac{1}{\sqrt{2}}e^{i\phi}\sin\theta\cos\tfrac{1}{2}\theta\times\sum_{l=1}(B_{l+}-B_{(l+1)-})(P_l''-P_{l+1}''),$$
$$H_2=\sqrt{2}\cos\tfrac{1}{2}\theta\sum_{l=0}(A_{l+}-A_{(l+1)-})(P_l'-P_{l+1}'),$$
$$H_3=\frac{1}{\sqrt{2}}e^{2i\phi}\sin\theta\sin\tfrac{1}{2}\theta\times\sum_{l=1}(B_{l+}+B_{(l+1)-})(P_l''+P_{l+1}''), \qquad (9)$$
$$H_4=\sqrt{2}e^{i\phi}\sin\tfrac{1}{2}\theta\sum_{l=0}(A_{l+}+A_{(l+1)-})(P_l'+P_{l+1}'),$$

where P_l' and P_l'' are first and second derivatives of Legendre polynomials.

The helicity elements are related to the electric and magnetic multipole elements as follows:

$$A_{0+}=E_{0+}, \quad A_{1-}=M_{1-},$$
$$\left.\begin{aligned}A_{l+}&=\frac{l+2}{2}E_{l+}+\frac{l}{2}M_{l+}\\ B_{l+}&=E_{l+}-M_{l+},\end{aligned}\right\}l\geq 1 \qquad (10)$$
$$\left.\begin{aligned}A_{l-}&=\frac{1-l}{2}E_{l-}+\frac{1+l}{2}M_{l-}\\ B_{l-}&=E_{l-}+M_{l-},\end{aligned}\right\}l\geq 2$$

where $E_{l\pm}$ and $M_{l\pm}$ are the parameters defined by CGLN.[29]

[28] The notation and normalization of the A's and B's is taken from Jean Hebb, who first introduced them.

[29] G. F. Chew, M. L. Goldberger, F. E. Low, and Y. Nambu, Phys. Rev. **106**, 1345 (1957).

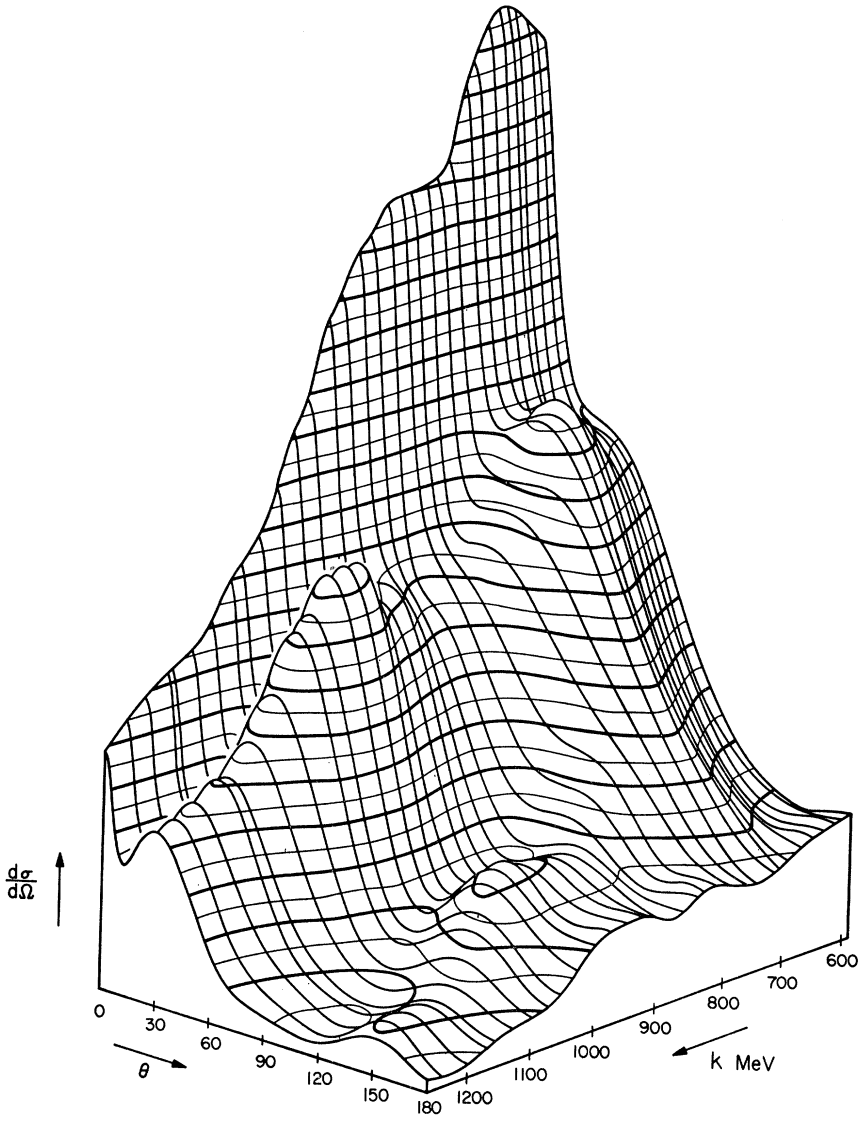

FIG. 4. An isometric view in which the 32 angular distributions, represented by the fitted curves (Fig. 3) are displayed as a function of π^+ c.m. angle and lab photon energy. Contours of constant differential cross section are drawn every 0.5 μb/sr, with alternate contours darker. The foremost double bump at 1000 MeV is the third resonance region. The second resonance peak occurs near 700 MeV.

From Eqs. (7) and (9), it may be shown that the interference of the OPE with other states for which $j \leq m$ has the form (note m is half-integral)

$$\sum_{n=1}^{4} \mathrm{Re}(H_n{}^{\mathrm{OPE}} H_n) \propto \frac{\sin^2\theta}{1-\beta\cos\theta} \times [b_0 + b_1\cos\theta + \cdots + b_{m-1/2}(\cos\theta)^{m-1/2}]. \quad (11)$$

The cross section from H_n alone is in general a polynomial in $\cos\theta$ of order $N=2m$. However, if only one parity of the highest j state is present, the order is $N=2m-1$. The entire cross section can therefore be written in the form

$$\sigma(\theta) = A\sigma_{\mathrm{OPE}}(\theta) + B\sigma_I(\theta) + \sum_{l=0}^{N} C_l P_l(\cos\theta), \quad (12)$$

where A and B are constants and not the helicity amplitudes, $\sigma_{\mathrm{OPE}}(\theta)$ is given by Eq. (8) with $\bar{G}^2/4\pi = 14.7$, and

$$\sigma_I(\theta) = \sin^2\theta\left(\frac{1}{1-\beta\cos\theta} - \frac{1}{1+\cos\theta}\right). \quad (13)$$

It is easily shown that the interference terms given by Eq. (11) are contained in Eq. (12) if we make suitable choices of the coefficients B, C_0, C_1, $\cdots$, $C_{m+1/2}$. Note that the coefficients C_l with $l > m+\frac{1}{2}$ are free of interference terms involving the OPE amplitude. The particular form of $\sigma_I(\theta)$ chosen is of course not unique; we have chosen a form which nearly vanishes except at small angles. We have used Eq. (12) to fit the angular distributions by varying the coefficients A, B, and C_l and also by varying B and C_l, with A fixed at $A=1$.

We have deviated from the usual form of the Moravc-

TABLE IV. Results of variable coupling-constant fits. At each photon energy k (in MeV), $G^2/4\pi$, and χ^2, divided by the number of degrees of freedom, are given for several orders of fit. Δ is the standard uncorrelated error in $G^2/4\pi$. Errors correlated with other coefficients are not indicated. N specifies the order of fit, the highest Legendre polynomial being $P_N(\cos\theta)$. The values of N chosen to obtain the average coupling constant are marked with an asterisk (*).

k	N	χ^2/d	$G^2/4\pi$	Δ	k	N	χ^2/d	$G^2/4\pi$	Δ	k	N	χ^2/d	$G^2/4\pi$	Δ	k	N	χ^2/d	$G^2/4\pi$	Δ
589	*2	1.0	19.9	2.5	603	*2	1.1	21.1	2.5	618	*2	0.8	25.1	2.5	635	2	1.4	22.6	2.5
	*3	0.9	15.9	3.5		*3	1.2	20.7	3.4		*3	0.6	20.9	3.4		*3	1.0	15.6	3.4
	4	1.0	15.5	5.1		4	1.0	13.0	4.9		4	0.7	21.0	4.9		4	1.0	11.1	4.8
	5	1.0	9.4	7.2		5	1.1	10.8	7.0		5	0.7	16.9	6.9		5	1.0	6.9	6.8
647	2	1.8	22.2	2.0	663	2	1.0	25.3	2.0	680	2	1.6	23.9	2.0	698	2	1.2	21.0	1.9
	*3	1.5	16.8	2.8		*3	0.9	21.5	2.7		*3	1.5	20.6	2.7		*3	1.0	16.6	2.7
	*4	1.4	10.9	4.0		*4	0.7	15.6	3.9		*4	1.3	14.5	3.8		*4	0.5	8.1	3.7
	5	1.3	3.6	5.6		5	0.6	9.2	5.5		5	1.3	12.1	5.4		5	0.5	4.1	5.2
715	2	1.3	18.3	2.5	733	2	1.2	15.0	2.4	752	2	1.5	13.2	2.3	772	2	1.0	13.8	2.2
	*3	1.3	15.7	3.4		*3	1.2	11.3	3.1		*3	1.6	13.2	3.0		*3	0.8	17.9	2.9
	*4	1.1	9.6	4.4		4	1.1	6.7	4.2		4	1.6	9.3	4.0		4	0.8	14.9	3.8
	5	1.1	3.7	6.4		5	1.1	10.8	6.0		5	1.5	1.4	6.0		5	0.7	10.9	5.7
793	*3	1.6	14.8	2.3	813	*3	1.6	15.4	2.2	834	3	1.7	20.9	2.2	857	3	1.0	19.6	2.1
	4	1.4	19.5	3.1		4	1.4	19.9	3.0		4	1.6	24.7	3.0		4	1.0	16.6	2.9
	*5	0.9	9.4	4.5		*5	0.9	10.1	4.3		*5	1.0	14.8	4.2		*5	0.6	8.7	4.1
	6	0.9	13.4	6.2		6	0.9	11.8	6.0		6	1.1	15.1	5.8		6	0.6	9.0	5.5
880	3	1.4	21.7	2.3	902	3	1.8	26.7	2.2	926	3	2.8	28.6	2.2	951	3	3.7	30.1	2.2
	4	1.2	17.5	3.1		4	1.5	22.4	3.0		4	2.1	21.7	3.0		4	3.2	23.5	2.9
	*5	0.8	10.5	4.3		*5	0.6	11.3	4.2		*5	0.7	8.4	4.1		*5	1.2	8.1	4.1
	6	0.9	7.6	6.0		6	0.6	10.1	5.9		6	0.7	9.7	5.8		6	1.3	6.9	5.7
977	4	4.5	22.8	2.1	1002	4	3.4	25.9	2.0	1028	4	3.0	22.0	1.9	1056	4	1.4	24.9	1.8
	*5	1.4	7.3	2.8		*5	1.7	15.1	2.7		*5	1.3	11.7	2.6		*5	1.0	19.6	2.4
	*6	1.2	12.2	3.6		*6	1.4	21.0	3.4		*6	1.4	11.4	3.3		*6	1.0	19.5	3.1
	7	1.1	6.2	4.6		7	1.5	21.6	4.4		7	1.4	7.7	4.2		7	1.0	17.2	4.0
1074	4	2.7	22.4	1.8	1102	4	2.0	17.4	1.6	1131	4	3.1	15.5	1.5	1162	4	2.3	18.5	1.4
	*5	2.0	15.9	2.4		5	2.0	15.1	2.2		5	3.1	13.6	2.0		5	2.4	19.1	1.9
	*6	1.5	9.2	3.1		*6	1.7	10.2	2.9		*6	2.0	5.4	2.6		*6	1.4	11.8	2.5
	7	1.6	8.2	3.9		7	1.8	10.8	3.6		7	2.1	5.9	3.3		7	1.3	14.3	3.1
1174	4	2.1	17.2	2.8	1204	4	3.1	11.2	2.7	1235	4	4.3	13.5	2.6	1269	4	1.4	22.2	2.7
	5	2.0	21.5	3.7		5	1.7	21.6	3.5		5	2.7	24.5	3.4		5	1.3	26.1	3.5
	*6	1.3	10.0	4.9		*6	0.9	11.0	4.6		*6	1.5	12.0	4.4		*6	1.1	20.5	4.4
	7	1.3	11.9	5.9		7	1.0	11.0	5.5		7	1.3	18.0	5.4		7	1.2	19.1	5.6

sik fit,

$$\sigma(\theta)=(1-\beta\cos\theta)^{-2}\sum_{l=0}^{N+2}a_l\cos^l\theta, \qquad (14)$$

in order to facilitate interpretation of the results of the fit, namely the coefficients. The two types of fit are mathematically equivalent.

B. Fits with Variable Coupling Constant

If we vary the coefficient A in fitting an angular distribution with Eq. (12), the resulting value of A provides a "measurement" of the π-N coupling constant which is based on the high-angular-momentum components of $\sigma_{\mathrm{OPE}}(\theta)$. The values of $G^2/4\pi$ obtained for fits of various orders are given in Table IV. It was seen that the dependence of $G^2/4\pi$ on the order of fit is significant. Therefore, the choices of N at various energies are critical when obtaining a best average value.

There are several possible reasons for the dependence of $G^2/4\pi$ on N. First, we should notice that it is only the high partial waves in σ_{OPE} that determine A or $G^2/4\pi$. This is obvious since the lower partial waves are independently varied by the C_l. Consequently, any error in the data or in the form of Eq. (12) involving the high partial waves will give erroneous results. Since we have not explicitly included meson and baryon exchanges, other than the OPE, the possibility that Eq. (12) is inadequate exists. The dependence on N could arise since with higher N the approximation that the other poles are represented by polynomials is better. To check for this effect, we tried introducing a pole due to ρ meson exchange. Neither a significant decrease in χ^2 nor a necessary nonzero ρ pole amplitude was discovered.

Intermediate-state diagrams or resonances can also add uncertainties to the choice of N. Consider, for example, the region of the second resonance $D_{13}(1519)$. The cross section due to a $D_{3/2}$ state (A_{2-} and B_{2-}) has terms only up to $\cos^2\theta$, so at first hand $N=2$ seems sufficient. However, the third resonance $F_{15}(1688)$ is only 1.7 widths away. A $D_{3/2}-F_{5/2}$ interference is therefore expected which gives a $\cos^3\theta$ contribution. In addition, the fourth resonance $F_{37}(1950)$ is about 2.5 widths away from the second, and an $F_{7/2}-D_{3/2}$ interference gives a $\cos^5\theta$ contribution to the cross section. Hence, choosing $N=2$ or even 3 is an approximation which neglects the presence of the tails of the higher resonances. The fact that these terms are not quite small enough to be completely neglected causes χ^2 to decrease slowly with increasing N.

We were unable to make a decisive choice of N at each energy. In quoting a best average of $G^2/4\pi$, we increase its error to account for this uncertainty. The values of

TABLE V. The total cross section and the 0° and 180° differential cross sections given by the fixed $G^2/4\pi$ fits are tabulated versus laboratory photon energy k and total c.m. energy W.

k (MeV)	W (MeV)	σ_T (μb)	$\sigma(0°)$ (μb/sr)	$\sigma(180°)$ (μb/sr)
589	1409	84.44±0.84	19.63±0.56	3.08±0.29
603	1418	85.59±0.83	19.74±0.55	2.80±0.31
618	1428	87.27±0.85	20.66±0.57	3.10±0.31
635	1439	89.62±0.89	19.93±0.56	2.94±0.30
647	1447	92.33±0.77	20.62±0.44	2.89±0.29
663	1457	95.27±0.78	21.10±0.44	2.84±0.29
680	1468	99.84±0.79	20.71±0.43	2.34±0.29
698	1480	101.42±0.80	19.70±0.42	2.78±0.28
715	1491	103.03±0.93	19.53±0.55	2.40±0.29
733	1502	95.60±0.89	17.33±0.53	2.08±0.28
752	1514	85.62±0.89	17.09±0.51	2.24±0.27
772	1526	76.49±0.81	17.14±0.50	1.96±0.27
793	1539	65.36±0.64	16.81±0.42	2.69±0.25
813	1551	58.31±0.62	17.16±0.41	2.59±0.25
834	1564	52.66±0.58	17.29±0.40	2.40±0.23
857	1577	49.26±0.54	16.26±0.39	2.16±0.23
880	1591	48.94±0.62	16.18±0.43	2.03±0.23
902	1604	49.70±0.61	15.07±0.41	2.25±0.22
926	1618	50.62±0.61	15.00±0.40	2,46±0.21
951	1632	51.62±0.61	12.79±0.38	2.41±0.21
977	1647	55.71±0.43	12.17±0.27	2.35±0.21
1002	1661	55.74±0.44	10.97±0.26	2.15±0.20
1028	1676	53.98±0.42	9.86±0.24	1.68±0.20
1056	1692	47.99±0.38	9.36±0.24	1.22±0.18
1074	1702	43.82±0.38	9.06±0.22	1.01±0.18
1102	1717	35.37±0.32	8.17±0.20	0.93±0.15
1131	1733	28.64±0.28	7.55±0.19	0.82±0.13
1162	1749	23.54±0.25	7.25±0.18	0.68±0.13
1174	1756	21.75±0.43	7.82±0.30	0.59±0.13
1204	1772	19.49±0.41	6.83±0.28	0.35±0.12
1235	1788	17.32±0.37	6.46±0.27	0.15±0.12
1269	1806	16.76±0.39	5.86±0.26	0.52±0.27

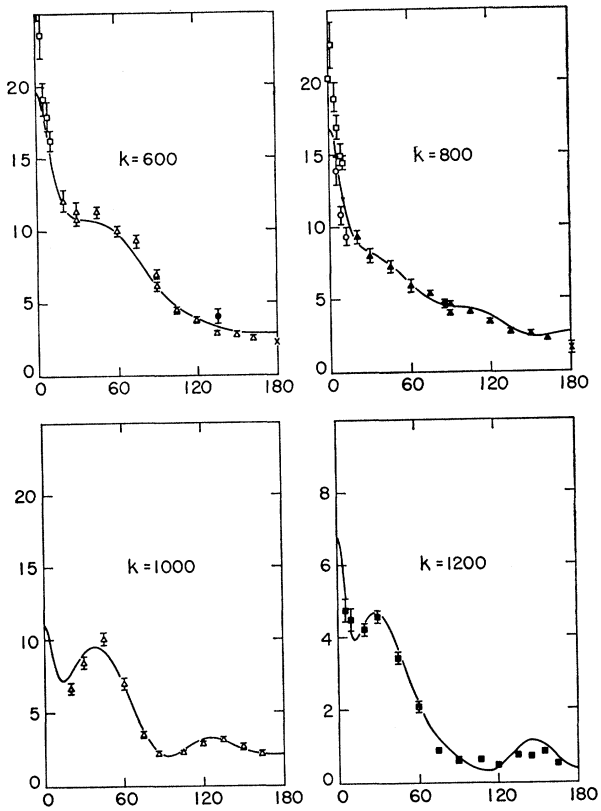

FIG. 5. The results of this experiment, represented by the smooth curves, are compared with the following data: □ Beneventano *et al.* (Ref. 18); ○ Boyden (Ref. 13); △ Dixon and Walker (Ref. 12); ▲ Dixon, Boyden (Ref. 13); ■ Kilner (Ref. 14); × L. Hand, C. Schaerf (Ref. 15); ● M. Heinberg *et al.* (Ref. 16).

N we selected are noted in Table IV. There are four regions of energy where we have allowed two values of N. Assuming N to vary systematically with energy, we will only consider averages of $G^2/4\pi$ over the 32 energies such that N is constant in each uncertain region. There are then 16 ways of taking the average corresponding to the different combinations of N for each region. We obtained in this way averages ranging from 12.7±0.6 to 15.6±0.6, with a median of the averages being 14.2. We therefore increase the error estimate to ±1.6 for our average. Adding the estimated systematic error of the experiment (4.3%) to this, our best value is

$$G^2/4\pi = 14.2 \pm 1.7 .$$

C. Fits with Fixed Coupling Constant

In order to investigate resonant states, the Moravcsik-equivalent fits were made with $G^2/4\pi$ fixed at a constant value of 14.7. This eliminates the fluctuations of the C_l with energy that are due to errors correlated with A. The coefficients C_l thus obtained depend upon the fixed value chosen for $G^2/4\pi$ only in a smooth manner which is slowly varying with energy. The coefficients are shown as functions of total c.m. energy in Fig. 6. The order of fit, N in Eq. (12), is 6. These fits are shown with the angular distributions in Fig. 3. The total cross sections obtained by integrating the fits and the 0° and 180° differential cross sections obtained from extrapolating the fits are given in Figs. 7 and 8, and in Table V.

VII. CONCLUSIONS

Several facts concerning the second and third resonance regions may be deduced from the coefficients C_l. By directly substituting the expressions for the helicity amplitudes [Eqs. (7) and (9)] into Eq. (6), and comparing with Eq. (12), it is possible to interpret some of the C_n in terms of the $A_{l\pm}$ and $B_{l\pm}$. Note from the comment made below Eq. (13) that if we neglect angular momentum states with $j>5/2$ in the H_n, then the coefficients C_4, C_5, and C_6 of the fit will be free of OPE interference terms.

The energy dependence of C_4 near $W=1688$ indicates the presence of at least one resonant state. It must have $j\geq 5/2$ to contribute to C_4. The possibility that it has $j>5/2$ is eliminated because no bump of the same magnitude is seen in C_6, and the 0° cross section, as we shall see, implies the production is almost entirely from a $B_{l\pm}$ amplitude, with initial helicity $\frac{3}{2}$. (For example, an $F_{7/2}$ state gives, in general, a cross section which is a sixth-order polynomial in $\cos\theta$. A fourth-order polynomial can occur if $|A_{3+}/B_{3+}|^2=26/4$, but such a ratio is ruled out

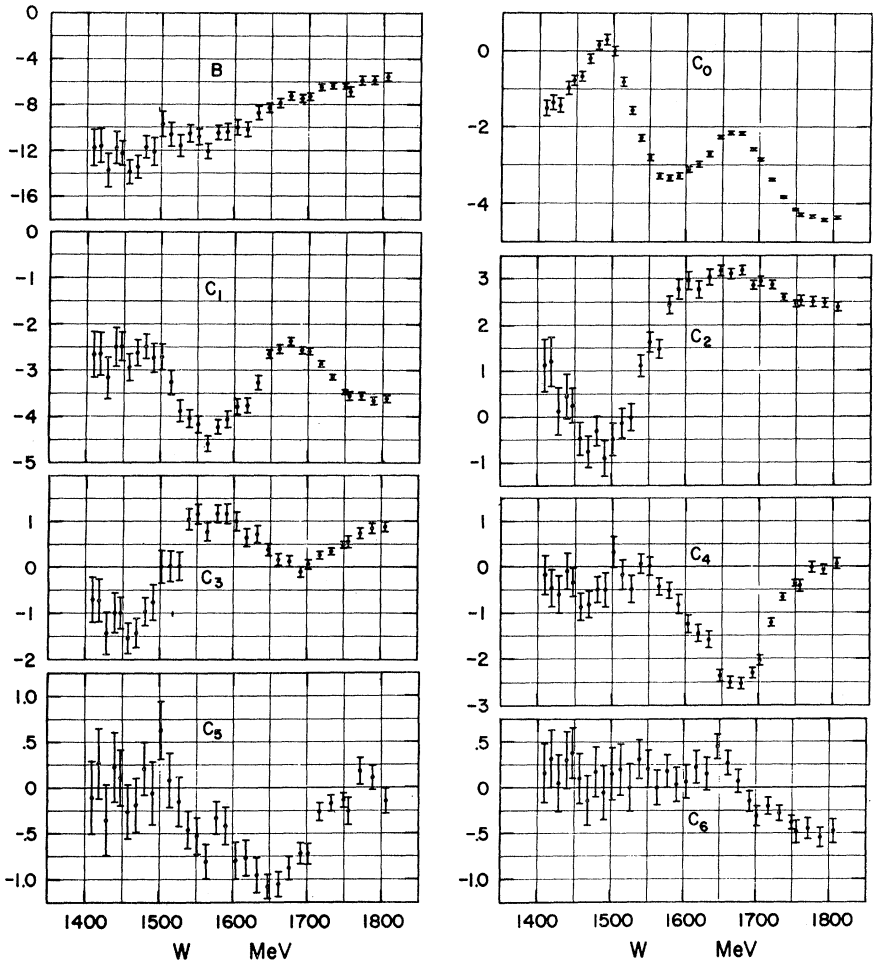

FIG. 6. The coefficients of the 32 Moravcsik-equivalent least-squares fits are given as functions of total c.m. energy W in MeV. The π-N coupling constant was fixed at the value 14.7. The coefficients are in units of μb/sr. C_l is the coefficient of $P_l(\cos\theta)$. B is explained in the text.

by the energy dependence of the 0° cross section.) According to C_4, the resonance can be either a $D(B_{2+})$ or an $F(B_{3-})$ wave, or a mixture of both.

The nonzero coefficient C_5 near $W=1688$ can only come from the interference of states of opposite parities. The only possibilities are a $D_{5/2}-F_{5/2}$ interference or interferences involving states with j greater than $\frac{5}{2}$. We reject the possibility of states with $j>5/2$ near 1688 MeV because no sign of them is seen in C_6. The energy dependence of C_5 is similar to a Breit-Wigner resonance shape, so it appears that there are both $D_{5/2}$ and $F_{5/2}$ resonances with nearly identical masses. Another alternative which gives a similar shape is for one of the states to be resonant and the other to be constant or slowly

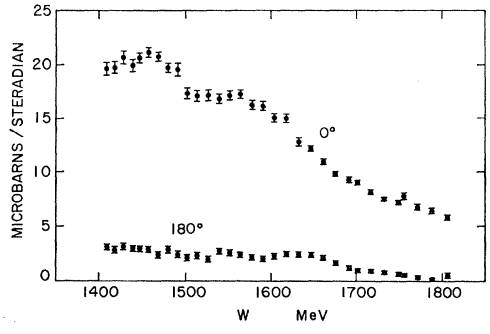

FIG. 7. Extrapolations of the Moravcsik-equivalent fits of the differential cross section to 0 °and 180° are plotted as functions of total c.m. energy.

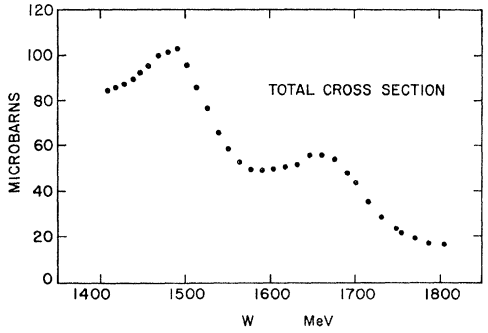

FIG. 8. The total cross sections, obtained by integrating the Moravcsik-equivalent fits, are plotted as a function of total c.m. energy.

varying, but with a predominantly imaginary amplitude. If we take both states to be resonances, the relative sizes of C_4 and C_5 give the relative magnitudes of the two resonances. In terms of their contributions to the total cross section at resonance, the ratio of smallest to largest is 0.07 ± 0.03, where the uncertainty results largely from uncertainties in the resonance masses and the nonresonant background. Which state is the larger cannot be decided *a priori* because of the symmetry of the cross section under parity. However, the energy dependence of C_3 indicates an interference between the second and third resonances and, with the usual $D_{3/2}$ assignment of the second resonance, this suggests the opposite parity state $F_{5/2}$ is the larger.

The indicated presence of a $D_{5/2}$ resonance is interesting in light of a quark model given by Moorhouse.[9] The model predicts the vanishing of direct photoproduction of the D_{15} from protons. The most likely conclusion from our data is that there is a finite but small D_{15} amplitude. It is apparently suppressed in photoproduction from protons compared to π-N scattering where its amplitude is about 0.6 of the F_{15} amplitude. A small finite photoproduction of D_{15} does not contradict the model since indirect production could occur, such as in a final-state interaction.

The second resonance (1519) shows up strongly in C_0 and C_2, consistent with its usual D_{13} assignment. The size of the peak in C_0 gives a peak total cross section of around 44 μb; however, the shape of the peak and attempts to fit C_0 and C_2 with Breit-Wigner forms plus nonresonant background, suggest that a good part of the bump is due to the nonresonant background. The resonant part alone could be as small as 24 μb at its peak ($W\approx1519$).

The coefficient C_6 shows the effect of the fourth resonance $F_{37}(1950)$ both by itself and as an interference with the third F_{15} resonance. The sign of C_6 indicates the fourth resonance is mainly produced by a state of initial helicity $\frac{3}{2}$ (B_{3+}). A Breit-Wigner form for B_{3+}, centered at $W\approx1950$ MeV, with a full width of 250 MeV and contributing a peak total cross section of 4.3 μb, will explain the C_6 coefficient.

An interesting conclusion concerning the second and third resonances follows from examination of the 0° and 180° cross sections in comparison to the total cross section. We see that whereas the bumps in the total cross section amount to 44 and 25 μb for the second and third resonances, respectively, the 0° and 180° cross sections show very little resonantlike energy dependence at the second resonance and none at all at the third. By conservation of angular momentum, an initial-helicity-$\frac{3}{2}$ state cannot contribute at 0° or 180°, whereas initial helicity $\frac{1}{2}$ does. We conclude therefore that the second resonance is mostly produced by the initial-helicity-$\frac{3}{2}$ amplitude (B_{2-}) and the D and F waves of the third resonance are almost entirely produced from initial-helicity-$\frac{3}{2}$ amplitudes (B_{2+} and B_{3-}). The $A_{l\pm}$ amplitudes are small for these resonances. This property of the second and third resonances, stated in terms of ratios of electric and magnetic multipoles, was first noticed by Beder[30] in π^0 photoproduction. However, the π^+ data at 0° and 180° provide a more sensitive measure of these ratios through interference with nonresonant amplitudes. A sum-rule calculation[1] gives, for the second and third resonances, ratios $A_{2-}/B_{2-}=0.04$ and $A_{3-}/B_{3-}=0.11$, respectively. These ratios are small enough to be consistent with our data.

The many states found in the phase-shift analysis of π-N scattering suggest there is more to look for in photoproduction. There are four resonances presently known or speculated to be present in π-N scattering which are not apparent in the coefficients C_l. If present in photoproduction, these resonances $P_{11}(1471)$, $S_{11}(1561)$, $S_{11}(1715)$, and $S_{31}(1692)$ are difficult to discover by the techniques employed here because of their low angular momentum and large widths. We certainly cannot say they are not present, at least in small amounts. In fact, the 0° cross section does appear to have bumps near 1471- and 1561-MeV total c.m. energy. All four of these resonances having $j=\frac{1}{2}$, if photoproduced, come from initial helicity $\frac{1}{2}$ and should be seen at 0° and 180°. The $S_{11}(1715)$, like the D_{15}, is predicted to be absent in photoproduction, according to a quark model.

ACKNOWLEDGMENTS

H. A. Thiessen carried out an experiment at backward angles complementary to this one. We are indebted to him not only for his data which were needed in fitting angular distributions, but for his part in the joint effort of computer programming, for his calibrations of the quantameter and the beam energy meter, and for numerous discussions. Frank Wolverton not only developed the theory and programs needed to compute the bremsstrahlung spectrum, but he also designed and tested the Freon gas Čerenkov counter which worked very well and was invaluable for this experiment. For the maintenance and operation of the synchrotron, we wish to thank the crew under Larry Loucks and the synchrotron operators under Al Neubeiser.

[30] D. S. Beder, Nuovo Cimento **33**, 94 (1964).